

## Chemistry on a Single Protein, Vascular Cell Adhesion Molecule-1, during Forced Unfolding\*

Received for publication, April 13, 2004, and in revised form, August 9, 2004  
Published, JBC Papers in Press, August 11, 2004, DOI 10.1074/jbc.M404103200

Nishant Bhasin<sup>‡</sup>, Philippe Carl<sup>‡</sup>, Sandy Harper<sup>§</sup>, Gang Feng<sup>¶</sup>, Hui Lu<sup>¶||</sup>, David W. Speicher<sup>§</sup>,  
and Dennis E. Discher<sup>‡§\*\*</sup>

From the <sup>‡</sup>Systems Biology and Polymer Engineering Laboratory, the Department of Chemical and Biomolecular Engineering, University of Pennsylvania, Philadelphia, Pennsylvania 19104, <sup>§</sup>Systems Biology Program, The Wistar Institute, Philadelphia, Pennsylvania 19104, and the <sup>¶</sup>Department of Bioengineering, University of Illinois, Chicago, Illinois 60607

**Proteins of many types experience tensile forces in their normal function, and vascular cell adhesion molecule-1 (VCAM-1) is typical in this. VCAM has seven Ig domains, and each has a disulfide bond (-S-S-) buried in its core that covalently stabilizes about half of each domain against unfolding. VCAM is extended here by single molecule atomic force microscopy in the presence or absence of reducing agents. In the absence of reducing agent, a sawtooth pattern of forced unfolding reveals an average period and total length consistent with disulfide locations in VCAM. With increasing reducing agent, accessible disulfides are specifically reduced (to SH); the average period for unfolding increases up to saturation together with additional metrics of unfolding. Steered molecular dynamics simulations of unfolding indeed show that the core disulfide bond is solvent-exposed in the very earliest stages of protein extension. Michaelis-Menten kinetics emerge with reduction catalyzed by force ( $\tau_{\text{reduction}} \sim 10^{-4}$  s). The results establish single molecule reduction, one bond at a time, and show that mechanical forces can play a key role in modulating the redox state of cell adhesion proteins that are invariably stressed in cell adhesion.**

For many cytoskeletal, adhesion, and matrix proteins, length and extensibility are considered central to function (1), and recently developed single molecule techniques using atomic force microscopy (AFM)<sup>1</sup> (2, 3) or other methods (4) offer novel insight. AFM allows stretching of individual proteins. This permits correlations of forced unfolding with structural determinants as well as ligand binding processes such as those sketched in Fig. 1. Common in extracellular proteins, disulfide bridges generally stabilize and limit unfolding. However, disulfides can also bind and react with reducing agents. Indeed, the reduced or oxidized state of a cell surface protein, such as

VCAM-1 studied here, is dictated by a cell surface microenvironment that can be far less oxidizing than commonly thought (5).

Single molecule experiments have already demonstrated patterns of forced unfolding for cell adhesion molecules (CAMs) (6), cell matrix proteins (7), and cytoskeletal proteins (2, 8). Multiple domains are the norm and clearly determine protein length (1) while probably also contributing to extensibility. CAMs mediate adhesion to neighboring cells or extracellular matrix and are stressed through the contractile or motile processes of cells and/or external forces (e.g. fluid shear). Of interest here is the Ig-type cell adhesion protein, VCAM-1, which is typical in having tandem Ig domains where each domain contains a disulfide bond hidden within its core (1). Of critical importance to the studies here, the core disulfide is inaccessible to reducing agent unless the Ig is exposed through unfolding by denaturant, temperature, or force (6). By forcibly extending VCAM in AFM under controlled reducing conditions, we demonstrate an ability to do covalent chemistry that is both specific and saturable on a single molecule during the relatively rapid process of forced unfolding. The biological implications of coupling redox chemistry to mechanical force are discussed.

VCAM is an especially important Ig-CAM in inflammatory function and vascular disease (9, 10). It is induced on endothelial cells by cytokines (11) and is found on smooth muscle cells and macrophages in atherosclerotic plaques (12). It can mediate adhesion of lymphocytes, eosinophils, or monocytes via the integrin  $\alpha_4\beta_1$ . VCAM has seven extracellular Ig domains, and each domain has one core, disulfide bond as described above. The first and fourth domains also have a second S-S bridge that appears solvent exposed in crystal structures (Fig. 2A). The color scheme of Fig. 2 highlights the fact that disulfide bonds typically bridge and lock away 50–60% of each domain (Table I). Unfolding about half of each domain can occur with the disulfide intact, regardless of reducing agent. However, if a reducing agent such as dithiothreitol (DTT) is present at high enough concentration and if it can reduce the disulfide to -SH fast enough, the unfolded length of a domain should double or more.

A similar five-domain IgCAM, MelCAM, in forced extension by AFM has already shown asymmetric sawtooth patterns of unfolding (6). 1 mM DTT was found to modulate length and period of the sawtooth pattern. As widely understood now, each peak in such patterns corresponds to forced unfolding of a domain in a chain extended under the AFM tip (Fig. 2B). Following each peak, the deflecting cantilever rapidly relaxes, and this is soon followed by nonlinear extension of the unfolded chain. Domains are unfolded in a sequence according to the unfolding force needed to cross over the energy barrier from

\* This work was supported by a National Institutes of Health (NIH) R01 grant (to D. E. D.), a National Science Foundation Presidential Early Career Award for Scientists and Engineers (to D. E. D.), and an NIH Bioengineering Research Partnership grant to the University of Pennsylvania Institute for Medicine and Engineering. The costs of publication of this article were defrayed in part by the payment of page charges. This article must therefore be hereby marked "advertisement" in accordance with 18 U.S.C. Section 1734 solely to indicate this fact.

|| Supported by a Whitaker grant to the University of Illinois Bioengineering Department.

\*\* To whom correspondence should be addressed. Tel.: 215-898-4809; Fax: 215-573-2093; E-mail: discher@seas.upenn.edu.

<sup>1</sup> The abbreviations used are: AFM, atomic force microscopy; CAM, cell adhesion molecule; VCAM, vascular cell adhesion molecule; DTT, dithiothreitol; SMD, steered molecular dynamics; TCEP, tris(2-carboxyethyl)phosphine.

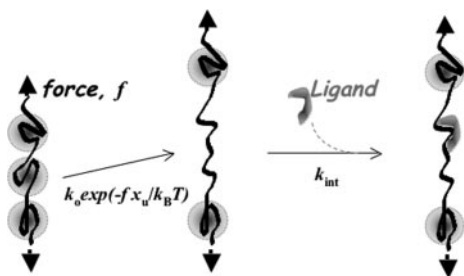


FIG. 1. Schematic of forced extension with a conformational change that allows ligand binding. Variables are fully defined under “Results.”

folded to unfolded rather than by the position of the domain in the chain (13). However, unfolding force depends on chain extension rate, which makes mechanical unfolding by AFM a kinetically driven process (14, 15).

Here we elucidate the forced unfolding of the Ig domains of VCAM and assess the relative kinetics of reducing core disulfides. Results from varying the reducing agent concentrations clearly indicate that increasing the reducing environment leads to an increased unfolding of domains with specific and saturable but rate-dependent reduction of core disulfide bonds.

#### EXPERIMENTAL PROCEDURES

**Steered Molecular Dynamics (SMD) Simulations**—Molecular dynamics simulations were carried out using the program NAMD (19) with the CHARMM22 force field (20). The x-ray structure of the first two domains of VCAM-1 (Protein Data Bank code 1VSC) consists of 196 residues. Amino acids 1–89 (domain 1) and 88–196 (domain 2) were separately used in unfolding simulations. Each VCAM domain was solvated in a sphere of water that covered the protein with at least four shells of H<sub>2</sub>O in all directions, as described previously (15, 21). The resulting structures of the protein-water system with about 22,000 atoms each were equilibrated separately for 1 ns at 300 K before the SMD was performed. The root mean square deviation of equilibrated structures from their respective crystal structures were less than 1.5 Å.

The SMD simulation was carried out with a constant velocity of 0.01 nm/ps by fixing the C $\alpha$  atom of the N-terminal amino acid of a domain and then applying harmonic forces to the C $\alpha$  atom of the C-terminal amino acid of that domain along the vector of the fixed atom to the pulled atom. This constant velocity SMD mimics the cantilever-based stretching of proteins in AFM. The SMD simulation stops when the system extends about 15 nm, at which point the disulfide bond between the cysteines of VCAM limits the domain from further extension.

A Linux cluster consisting of 10 2000+ Athlon processors was used for the simulation. The trajectories of the SMD simulations were obtained by saving the atomic coordinates of the whole system every 500 steps with each time step set to 1 fs. Analyses and display of molecular structures were done with VMD visualization software (22).

**Protein Preparation**—Recombinant extracellular domain of human VCAM-1 (R&D Systems), in which the seven extracellular domains are retained but the cytoplasmic tail and transmembrane region have been removed is used. The sample was concentrated in a 30-kDa cut-off Centricon concentrator (Millipore Corp.), and then, to remove any aggregates or fragments, it was purified by gel filtration using a Super SW3000 column (4.6 mm  $\times$  30 cm; Tosoh) equilibrated in 10 mM sodium phosphate, 130 mM NaCl, pH 7.4, and maintained at 4 °C. Mass spectrometry indicated a single species of the appropriate molecular weight. Sedimentation equilibrium was also performed to show that VCAM-1 is strictly monomeric.

For AFM experiments, protein was stored on ice, and any aggregates were removed before each experiment by centrifugation at  $166,000 \times g$  for 1 h at 4 °C. 50  $\mu$ l of protein-PBS solution (with or without reducing agent) at 0.1 mg/ml protein was allowed to adsorb for 15 min at room temperature onto a substrate of freshly cleaved mica. Excess protein was lightly rinsed away with the same PBS solution and placed without drying under the head of the AFM. AFM imaging after scratching the substrate surface was used to verify that only a monolayer of molecules covered the surface (6). In separate experiments, fluorescence imaging of labeled VCAM demonstrated homogeneous adsorption to the surface. Bridging configurations in which protein spanned the gap between substrate and AFM tip are dominant but desirably infrequent under

conditions of low surface coverage. Higher protein concentrations show higher unfolding force because multiple proteins will tend to attach to the tip and be stretched to unfold in parallel. We have shown this previously with a series of spectrin constructs (8), and the principle is the same as that long understood in studies of cell adhesion where large adhesive contacts at high concentrations of ligand-receptor pairs will generally yield forces of detachment that are much higher than the force required to break a single ligand-receptor bond (23). Thus, importantly, the mechanical stability of individual domains does not depend on the protein concentration, but working at the lowest possible protein concentration is necessary to obtain the unitary force for unfolding.

**Reducing Agents**—The fluid cell was filled with PBS plus or minus reducing agent, thus making sure that all measurements were carried out in a homogeneous oxidizing or reducing environment. Two different reducing reagents were used: DTT and tris(2-carboxyethyl)phosphine (TCEP).

**Dynamic Force Spectroscopy**—The AFM methods are largely the same as those in Ref. 8. Experiments were performed at 23 °C with imposed displacement rates of either 1 nm/ms or 5 nm/ms. Some refolding experiments were also done at 0.5 nm/ms.

Since bridging contacts and extension are stochastic and intrinsically random in many ways, collection and analyses of thousands of peaks is necessary to provide an accurate statistical view. For the majority of AFM experiments here, 6000 substrate contacts were made. As in Ref. 8, a custom analysis program was used to analyze the spectrograms with countable peaks identified when tip deflections exceeded 3 times the base-line fluctuations. Because results obtained in the first hour were similar to those obtained at the end of the experiment, denaturation of protein during the several-hour-long experiment could be ruled out.

**Changing Solutions Midexperiment**—To look at the stepwise effect of adding and removing reducing agent, the AFM protocol was changed as summarized in Table II. First, 3000 force spectrograms were obtained under standard oxidizing conditions (Stage I). DTT was then sequentially introduced into the cell at the stated concentrations, and 3000 spectrograms were again collected under these (reducing conditions) (Stage II). Last, the DTT solution was replaced with iodoacetamide to acetylate any free -SH, and this was allowed to stand for 20 min. The iodoacetamide solution was replaced with PBS, and 3000 force spectrograms were recorded (Stage III). Dye experiments done in parallel to the actual experiment show about 80% washout of DTT after stage II. The results listed in Table II are discussed below.

#### RESULTS

**Forced Unfolding of VCAM: Experimental Scheme**—Forced unfolding of the first two Ig domains of VCAM is depicted schematically in Fig. 2B. In the absence of reducer, the force applied in AFM is understood to break key initial interactions (critical hydrogen bonds) (24) that then allow complete unfolding up to the intact disulfide bonds. Under reducing conditions with either DTT or TCEP in solution, these initial steps remain the same, but, as protein domains partially unfold, S–S bonds hitherto inaccessible to the aqueous medium become reduced. Continued application of force after reduction leads to more unfolding through disruption of a few more critical interactions (e.g. core hydrophobic interactions) and full unfolding. In this stepwise process, the reactivity of the disulfide bond to reducing reagents becomes useful for demonstrating the conformational stability of such proteins under force.

Ig domains in solution are known to require some kind of denaturant along with reducing agent for such complete unfolding (6, 25, 26). The force applied by AFM acts as a “physical denaturant” here. If the domain fluctuates so as to expose the disulfide bond to solvent, however, the disulfide bond would be reduced even in the absence of denaturant. As an example, the native  $\beta_2$ -microglobulin Ig-type domain reportedly experiences global fluctuations that expose the core disulfide bond, thus allowing complete unfolding with reduction even in the absence of denaturant (25). However, our earlier studies on the IgCAM protein MelCAM, which is more closely related to VCAM than  $\beta_2$ -m, demonstrate that core S–S are solvent-inaccessible (6). The saturation kinetics for reduction shown in the present study will significantly extend our understanding of the rela-

**FIG. 2. Forced extension with reduction of VCAM-1 by AFM.** *A*, the extracellular structure of VCAM contains seven Ig domains. Disulfide bonds are shown in red. The yellow and white ribbon structure of the first two repeats of VCAM (Protein Data Bank number 1VSC) shows the disulfide-delimited cores in yellow. The other five repeats schematically indicate the core locations of disulfides, with yellow segments indicating unfoldable structures only under reducing conditions. For the experiment, the protein is adsorbed to freshly cleaved mica, and nonadsorbed protein is washed away. *B*, experimental AFM set-up and proposed reduction-coupled mechanism for forced unfolding of the first two VCAM repeats. From state *i* to state *ii*, the intradomain disulfide bonds are first exposed by force and then reduced.

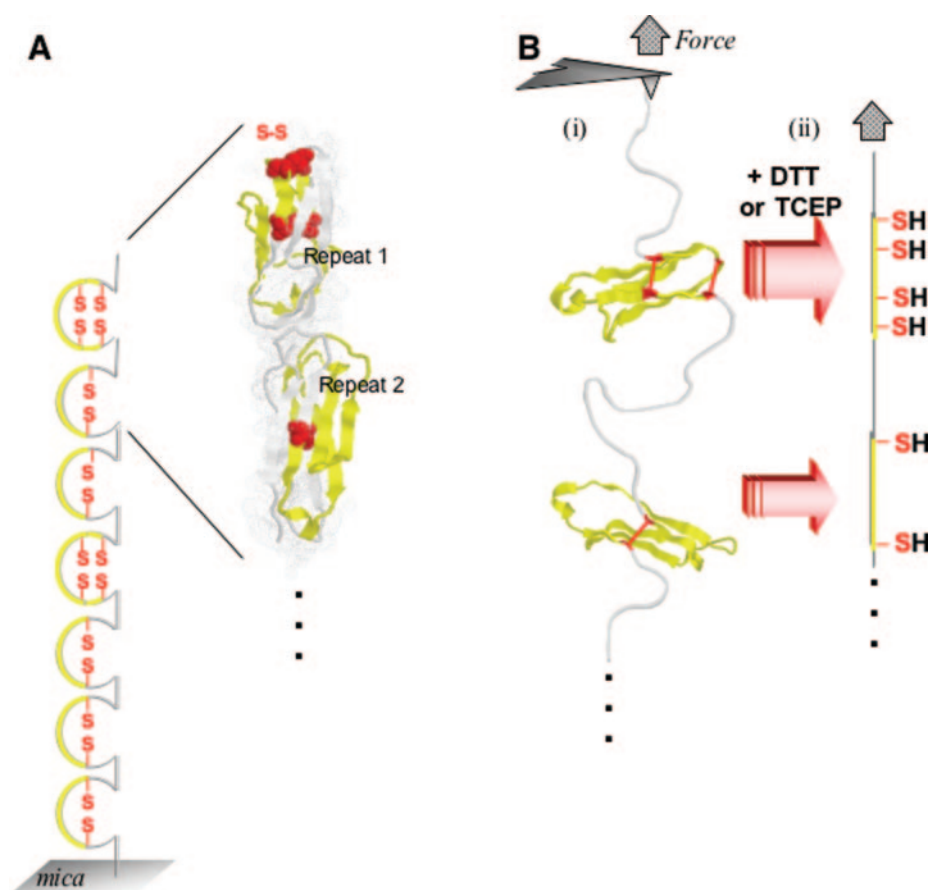


**TABLE I**  
Key structural features of VCAM-1 extracellular Ig domains

Individual domains	Number of aa <sup>a</sup> outside Cys	Oxidized contour length	Total number of aa	Reduced contour length
		<i>nm</i>		<i>nm</i>
1	37	13.7	90	33.2
2	44	16.2	103	38.0
3	46	17.0	92	34.0
4	40	14.8	93	34.3
5	44	16.2	103	38.0
6	46	17.0	92	34.0
7	47	17.3	93	34.3
Average	43.4	$\langle l^O \rangle = 16.0$	95.1	$\langle l^R \rangle = 35.1$
Total		$L_C^O = 111.2$		$L_C^R = 245.8$

<sup>a</sup> aa, amino acids.

**TABLE II**  
Unfolding length per peak extension for a three-stage experiment with iodoacetamide capping of any reduced disulfides

Stage	DTT	DTT removed, iodoacetamide added	Residual DTT after iodoacetamide	Unfolding length per peak extension
	<i>mM</i>	<i>mM</i>	<i>mM</i>	<i>nM</i>
I	0			20.9 ± 0.4
II	1			25
	5			30.8 ± 0.8
III	5	5	~0.8	25.2 ± 0.1

tive roles of tensile stress and reducing environment on the unfolding of Ig domains containing disulfide bonds.

**Simulated Unfolding Reveals Early Exposure of the Disulfide Bond**—Steered molecular dynamics simulations were performed on VCAM domains 1 and 2, starting with thermal equilibration of an available crystal structure. Applying force at one terminus while keeping the other end fixed gave force-

extension curves typical of many other proteins (15, 21, 24). A dominant unfolding barrier at around 2 nm of extension was seen for both domains; beyond this, the domains unraveled with much less resistance.

Snapshots in Fig. 3 show VCAM domain 2 under increasing end-to-end extension during forced unfolding. In the initial state, the disulfide bond between Cys<sup>113</sup> and Cys<sup>171</sup> (red) is buried in the center of the equilibrated domain. During stretching, the white-colored, outer strands from residue 86 (N terminus) to 113 and also from residue 171 to 196 (C terminus) are pulled away from the domain. In comparison, the yellow-colored segment of chain from residue 113 to 171 stays very well folded because of the disulfide bond. Note that if denaturants or heat were used on such a domain under nonreducing conditions, both yellow and white regions would unfold and appear very different. Forced unfolding, being vectorial, clearly peels away the outer strands, leaving the core intact. Refolding back onto this core should be facile as suggested in experiments below.

Importantly, at an extension of just 0.28 nm the core disulfide is exposed through a newly formed “pore” into the core. This can be clearly seen in Fig. 3. The size of this pore does fluctuate, but it does tend to grow as the overlying strands (white) are pulled away. These  $\beta$ -strands are fully unfolded at nearly 15-nm extension, but the disulfide bond appears maximally exposed by about half the full extension. SMD simulation of domain 1 shows similar behavior, with the disulfide bond clearly exposed at similar end-to-end extensions. Detailed trajectory analysis, measurement of the pore size along the unfolding trajectories, and comparisons between VCAM and other IgCAMs during unfolding will be presented elsewhere. What the molecular dynamics simulations clearly show, however, is that the core disulfide bond is exposed very soon after unfolding initiates. Provided the reduction reaction is sufficiently rapid,

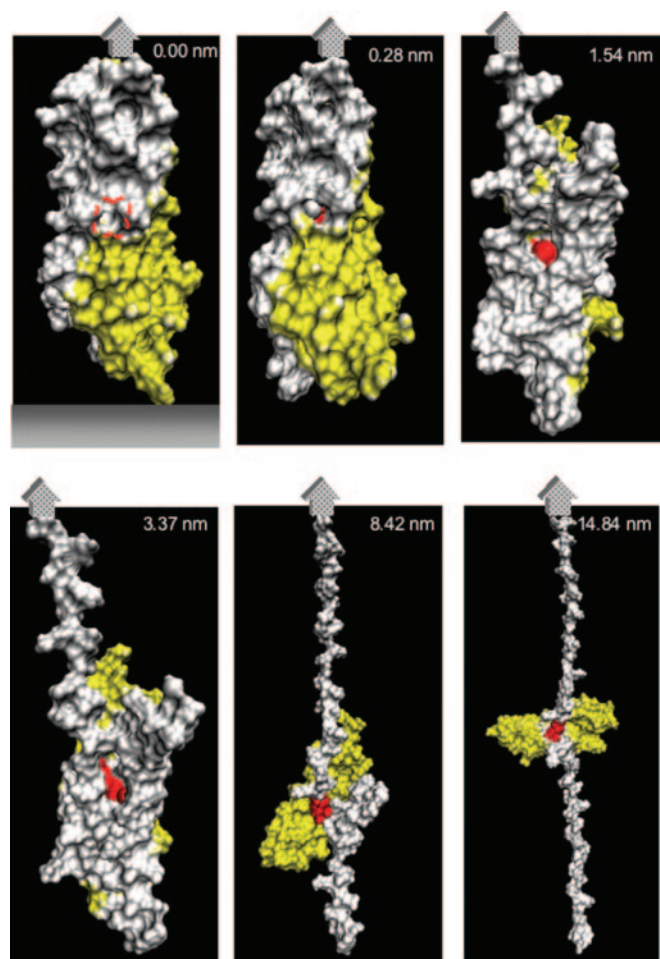


**FIG. 3. Simulation snapshots of the second domain of VCAM-1 in forced extension.** Surface rendering shows the disulfide bond between Cys<sup>113</sup> and Cys<sup>171</sup> in red, with the red dashed outline in the first panel indicating that the Cys residues are buried. In yellow are residues between 113 and 171 that are “locked away” by an intact disulfide, whereas in white are residues 86–112 and residues 172–196 that are extensible even under oxidizing conditions. The number at the upper right corner of each panel gives the extended length (in nm) of the domain. The relative size of the pore in each panel can be estimated from the exposure of Cys<sup>131</sup> and Cys<sup>171</sup>.

conversion of the S–S to S–H, giving a fully unfoldable domain, can therefore occur well before full extension. Experiments below demonstrate this.

**Sawtooth Patterns of Forced Unfolding: Overextension with S–S Reduction**—AFM extension experiments on VCAM were performed after it was first adsorbed onto a mica surface from dilute solution. An AFM cantilever tip with a radius (~20 nm) similar to the length of VCAM (~30 nm based on estimates from Fig. 2A) was then used to pick up single molecules by physisorption to the tip. When DTT and TCEP were used, their concentrations were  $\geq 1$  mM, for which there is on average  $\geq 1$  molecule of reducing agent/10 nm<sup>3</sup> of solution. Trialkylphosphines such as TCEP are highly specific for disulfides and reduce S–S more rapidly than does DTT (16). In addition to being water-soluble, TCEP is also highly stable in basic solutions (17), unlike DTT, which readily oxidizes above pH 7.5. The mechanisms for reduction of disulfide bonds with both TCEP and DTT are shown in Fig. 4 (18).

Forced extension of the bridging protein under both reducing and oxidizing conditions gave extension curves that showed quasiperiodic sawtooth patterns (Fig. 5, A and B). Such curves are consistent with a multidomain tertiary structure in sequential unfolding. After unfolding, work against the entropic elas-

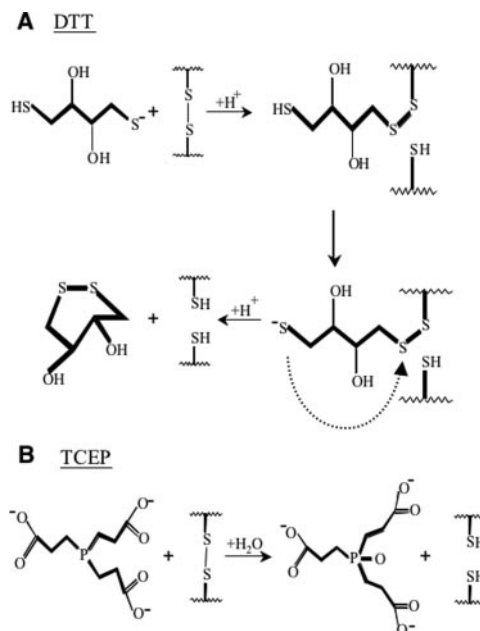


**FIG. 4. Mechanisms for disulfide bond (S–S) reduction in the presence of DTT (A) and TCEP (B).**

ticity of the unfolded protein is responsible for the rising slope of each peak in the sawtooth pattern. Such patterns are similar in form to results obtained for a wide range of proteins including MelCAM (6) and titin (2) but are not apparent in forced extension of either unstructured synthetic polymers (28), RNA, or DNA (29). We provide below a large scale statistical analysis of sawtooth patterns that show the disulfide bridges in VCAM Ig domains are intact as expected under oxidizing conditions (Fig. 5A), but they are increasingly disrupted under increased reducing conditions (Fig. 5B) up to saturation.

Regardless of conditions, force peaks are found to be much smaller than the unfolding forces reported for either titin (2) or fibronectin FNIII (7); the unfolding forces of VCAM are similar to those reported for the other disulfide-linked IgCAM studied previously, MelCAM, for which forces of ~30–50 piconewtons at similar rates of extension (0.01–10 nm/ms) were found (6). As with all such proteins, the exponentially increasing portions of the force-extension curves are reasonably well fit by a worm-like chain model for entropic elasticity (2) of an unfolded chain up to the point where another domain in the chain unfolds. As with MelCAM in 1 mM DTT, the addition of reducing agent (TCEP in Fig. 5B) clearly tends to increase the number of peaks ( $N_{pk}$ ) and the total extended length of VCAM in unfolding. Less obvious, but borne out in the statistics below, is the fact that the spacing between peaks tends to increase as reducer is added, but this effect is nonlinear and visible in Fig. 5 only at high reducer concentration. At low reducer concentration, reduction is not fast enough, and two-stage unfolding of each domain occurs. This is a key point of the study and is further discussed below.

**Reversible Unfolding under Oxidizing Conditions and Removal of the Reducer**—An initial indication of reversible unfolding was sought under oxidizing conditions. A single protein was extended more than one peak beyond the first desorption peak but well before final desorption (Fig. 5C), and then the extension was reversed before extending the protein again. Regular and well spaced force peaks in the repeated unfolding-refolding cycles correspond to unfolding lengths of single repeats and were recorded using different surfaces. As interpreted before by Rief *et al.* (2), the results indicate that some of the domains unfolded in the first extension of protein had

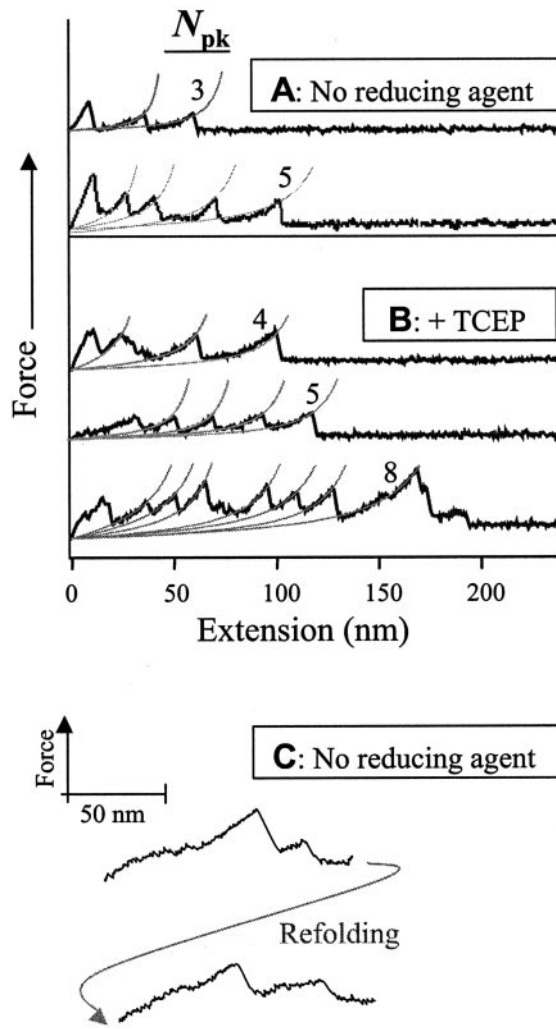


FIG. 5. **Representative force-extension curves.** Shown are unfolding curves for VCAM under oxidizing conditions (A), and reducing conditions (B) with 1–10 mM TCEP. The *first* and *last* peaks are identifiable as initial desorption from the surface and final desorption from the tip or surface, respectively; this is known from past studies of two-, three-, or four-repeat spectrin constructs, which showed up to four, five, or six peaks in AFM extension (8). Here, various numbers of unfolding peaks ( $N_{pk}$ ) are also shown; and more  $N_{pk}$  are clearly observed when VCAM is reduced. The rise phase in each sawtooth corresponded to extension of unfolded chains and was fit by the Worm-like chain (WLC) model (2, 27) for peaks beyond the first (8). The imposed rate of extension for all of the results shown was 1 nm/ms. C, sawtooth pattern for repeated stretching and relaxation of a single VCAM protein (at 0.5 nm/ms).

spontaneously refolded on relaxation. Internal interactions within protein domains thus prevail over protein-surface interactions.

A second set of experiments involved adding DTT and then removing it (see “Materials and Methods”; Table II). This was done in order to verify that the disulfide reduction was initiated only when coupled with AFM-forced extensions. Results for the extension length per peak,  $l$ , increased with reducing agent (5 mM DTT) but then decreased when DTT was removed to just a residual level (0.8 mM DTT). The results here are in accordance with results below (*i.e.* length statistics) and demonstrate essentially no reduction and no unfolding on the surface until VCAM is extended by AFM. While consistent with MelCAM, our observation contrasts with unfolding of pentadomain human angiotatin (30). The differences may indicate stability differences, or the 50 mM DTT used on angiotatin may be sufficiently excessive that DTT would gain access through angiotatin fluctuations

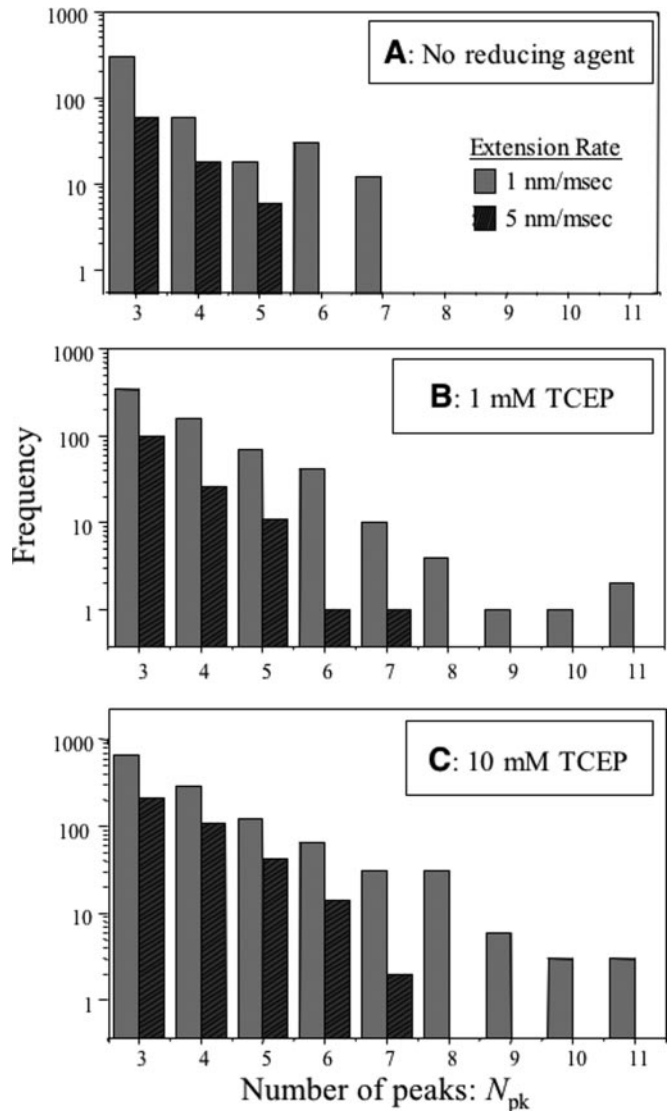


FIG. 6. **Histogram showing the frequency distributions for the number of force peaks observed under oxidizing (A) and reducing conditions with either 1 mM TCEP (B) or 10 mM TCEP (C).** The imposed extension rate was 1 nm/ms or 5 nm/ms, and the results are reported for 6000 contacts with protein adsorbed on substrate.

TABLE III

Percentage of spectrograms for each extension experiment with analyzable unfolding curves with either  $N_{pk} = 3$  or  $N_{pk} = 7$  for 6000 contacts (at 1 nm/ms)

VCAM-1	Percentage of spectrograms with	
	$N_{pk} = 3$	$N_{pk} = 7$
	%	%
0 mM DTT/TCEP	7.4	0.20
+ 1 mM DTT	5.3	0.22
+ 1 mM TCEP	10.5	0.30
+ 10 mM DTT	11.2	0.67
+ 10 mM TCEP	20.0	1.24

and reduce otherwise inaccessible S–S bonds.

**Peak Statistics of Forced Unfolding: Oxidized Versus Reduced**—Fig. 6 cumulates statistics on the number of visually countable force peaks  $N_{pk}$ . Under oxidizing conditions,  $N_{pk} \leq 7$ , but this increases considerably up to  $N_{pk} = 11$  under reducing conditions. The maximum number of peaks,  $\max(N_{pk})$ , is also seen to depend on the imposed extension rate  $v$  and tends to decrease with increasing  $v$ . In addition, the first and last peaks of any force sawtooth correspond to desorption events that

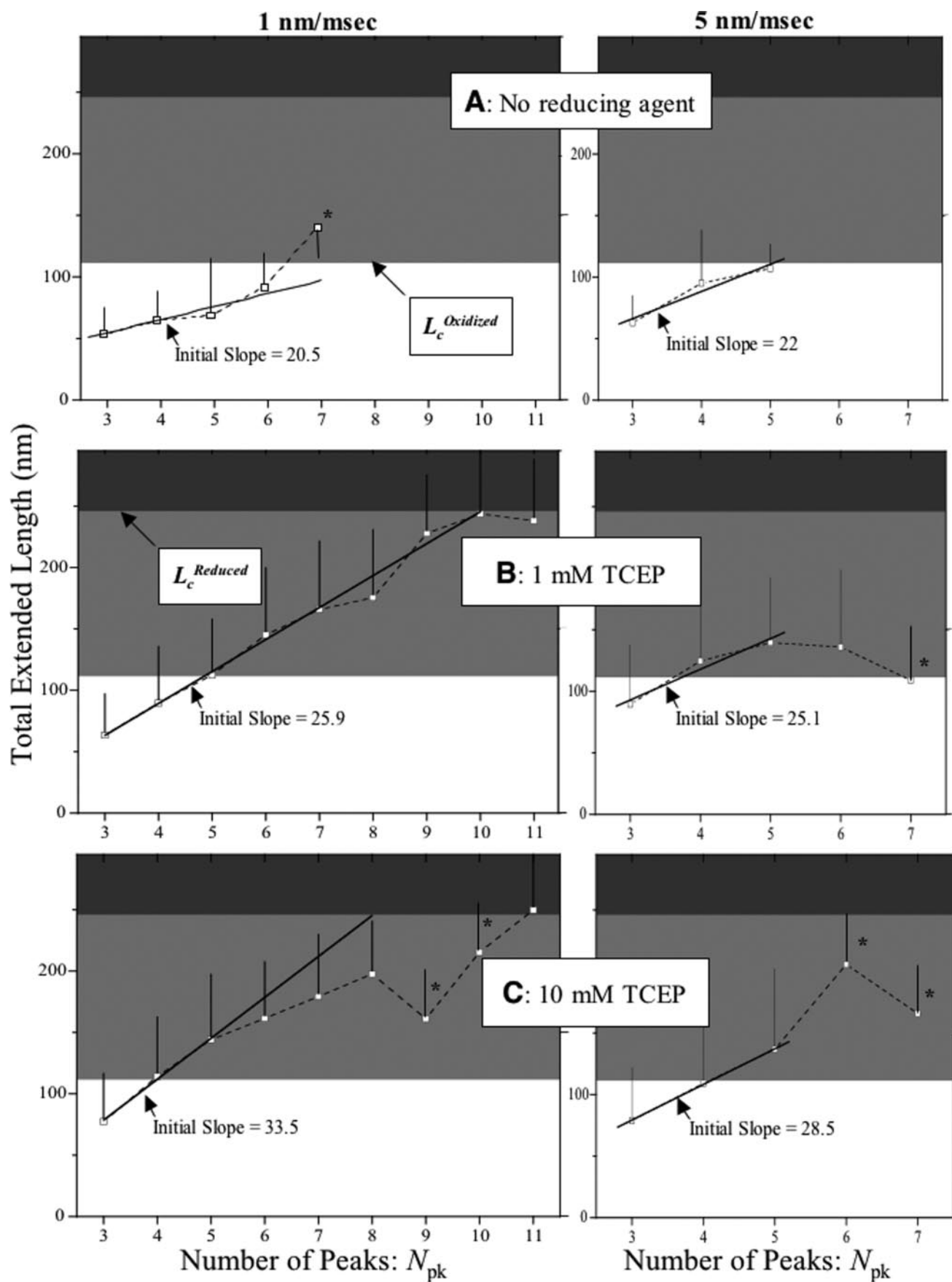


FIG. 7. Total unfolding length versus number of peaks observed for VCAM under oxidizing (A) and reducing conditions with either 1 mM TCEP (B) or 10 mM TCEP (C). Gray regions demarcate oxidized contour length ( $L_c^{Oxidized}$ ) and reduced contour length ( $L_c^{Reduced}$ ). Initial linear fits show trends for peaks ( $N_{pk} \leq 7$ ), which saturates thereafter. \*, averaging for  $\leq 2$  events.

TABLE IV  
Fits of data in Fig. 8, A and B, with  $l = l_0 + kX/(K + X)$

Reducing agent, X	Extension rate	$k$	$K$	$l_0$	Efficiency $\Phi = k/K$	$l_{\text{sat}} = l_0 + k$
	<i>nm/ms</i>	<i>nm</i>	<i>mM</i>	<i>nm</i>	<i>nm/mM</i>	
DTT	1	10.1	1.25	20.5	8.1	30.6
TCEP	1	15.1	1.75	20.5	8.7	35.6
TCEP	5	8.1	1.75	22	4.7	30.1

generally add two (8) to the number of domains,  $d_{\text{tot}}$  ( $d_{\text{tot}} = 7$  in Table I) for the expected  $\max(N_{\text{pk}})$ .

$$\max(N_{\text{pk}}) = d_{\text{tot}} + 2 \quad (\text{Eq. 1})$$

$N_{\text{pk}} > 9$ , as occurs with reduction, indicates partial unfolding of domains before and after reduction of individual disulfide bonds.

With increasing reducing agent, higher  $N_{\text{pk}}$  unfolding events tend to occur more frequently (Fig. 6). Since sawtooth patterns with  $N_{\text{pk}} \geq 3$  are indicative of unfolding (8), Table III enumerates the frequency of all such events under the various conditions. Increased reduction with increased reducer concentration as well as the increased reducing power of TCEP compared with DTT (at either 1 or 10 mM) are evident from Table III. The increase in unfolding events clearly reflects many more ways of unfolding under reducing conditions. Note that the cumulative percentages for  $N_{\text{pk}} \geq 3$  (*i.e.* all unfolding events) as tabulated in Table III are either within or well below single molecule measurement conditions that require success rates of  $\leq 20\%$  (31).

*Length Statistics of Forced Unfolding When Oxidized*—Plots of total extended length *versus* number of peaks (Fig. 7) prove even more revealing of the reducing effects. For high  $N_{\text{pk}}$ , the total extended length approaches the relevant contour length limit ( $L_c$ ), which is indicated by the *gray regions* in Fig. 7. These limits correspond to either oxidized (lower) or reduced (higher) VCAM and are calculated according to the peptide length and the amino acid sequence (Table I). Being well bounded by the known  $L_c$  of a single chain is also consistent with the lack of any multimeric VCAM aggregates, including artifactual inter-chain disulfide-linked structures that could form on the substrate if thiols from adjacent chains were exposed by unfolding.

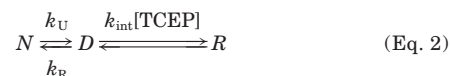
In all of the panels of Fig. 7, a straight line through the initial  $N_{\text{pk}}$  (up to 5 or more) generally provides an excellent fit. This initial slope represents a mean unfolded length per peak,  $l$ , which is reflective of processes occurring well below the contour limits. For the oxidized protein in Fig. 7 (*top panels*),  $l$  (equal to 20.5–22 nm) is much lower than the reduced contour length for any individual domain (see Table IV) and therefore suggests partial unfolding with intact core disulfides. This range of  $l$  nonetheless exceeds the average length expected from the domain sequence:  $\langle l^N \rangle = 16.0$  nm (Table I). We hypothesize that this partial unfolding can be attributed to a more complex propagation of unfolding of the linking structures between VCAM domains. Fig. 2A highlights the interlocking strands between adjacent domains 1 and 2. Such interactions would tend to induce linker unfolding and result in adjacent domains being partially unfolded. Consistent with this idea is the previous finding (Fig. 6A) that native chains show no more than five (equal to  $\max(N_{\text{pk}}) - 2$ ) unfolding peaks after accounting for the two desorption peaks (first and last). Furthermore,  $l \times (\max(N_{\text{pk}}) - 2) = 102.5$  nm compares very well with  $L_c^{\text{Oxidized}} (\approx 7 \langle l^O \rangle) = 111.2$  nm. The implication is that the seven Ig domains of VCAM behave mechanically as if there are just five domains, perhaps because of unfolding through linkers.

*Length Statistics of Forced Unfolding When Reduced*—Our

principal focus here is on the effects of reducing agents. Measured slopes  $l$  for the initial regime clearly increase with increasing concentrations of both TCEP (Fig. 7) and DTT. Extrapolating the initial linear fits to the relevant contour limit ( $L_c^{\text{Oxidized}}$  or  $L_c^{\text{Reduced}}$ ) is also revealing. In the absence of reducing agent, the extrapolated intersection  $\text{intx}(N_{\text{pk}}) \sim 7$ –8 implies  $(\text{intx}(N_{\text{pk}}) - 2) = 5$ –6, which is consistent with the five-domain mechanisms above. For 1 mM TCEP, this point of intersection is nearer  $(\text{intx}(N_{\text{pk}}) - 2) = 8$ , whereas for 10 mM TCEP, the intersection decreases back to  $(\text{intx}(N_{\text{pk}}) - 2) = 6$ . The initial extension behavior in each case, respectively, suggests the mechanical presence of five, eight, or six “domains.” The eight “detected” domains at 1 mM TCEP suggest some two-step unfolding wherein unfolding stops at the disulfide until TCEP reduces it (see Fig. 4B). At a higher TCEP of 10 mM, in contrast, the delay is minimized, and full unfolding is suggested to be so rapid as to be continuous with disulfide reduction.

As is typical of kinetic analyses (*e.g.* enzyme kinetics), we have analyzed just the initial slopes of the processes here. Different processes occur beyond the initial regime (*e.g.* substrate depletion with enzymes at long times). In Fig. 7C for  $N_{\text{pk}} > 5$ , for example, the results are below the initial linear fit, which implies that unfolding-reduction processes are sometimes more two-stage as at lower [TCEP]. The large number and complexity of intramolecular interactions within a protein molecule also make it likely that the reaction mechanism (and hence reaction order) change as successive domains are unfolded in a protein. Thus, in order to assess reaction order at its fastest rate during forced unfolding, the focus above was on  $l$  from the initial regime ( $N_{\text{pk}} = 3$ –6). This also seems reasonable because the fraction of events with  $N_{\text{pk}} > 6$  is comparatively low (Table III). This initial length  $l$  extended per peak/domain also provides an effective measure for the mean concentration of the unfolded state.

*Saturable and Specific Reduction*—Data in Fig. 7 can be explained by comparing the kinetics of reduction of the disulfide bond with the kinetics of unfolding and refolding. Past mechanisms (25) take the native state ( $N$ ) through a denatured state ( $D$ ) to a fully reduced state ( $R$ ) with multiple rates as indicated in the following.



In our experiments, due to very high pulling rates, we always operate in the irreversible range where  $k_U \gg k_R$ .

Fig. 8A plots the experimentally determined  $l$  *versus* [DTT] and then fits the results to Michaelis-Menten enzyme kinetics with the applied force playing the role of the catalyst, decreasing the energy barrier(s) and thus accelerating the reduction reaction in the standard Michaelis-Menten form.

$$l = l_0 + k[\text{DTT}]/(K + [\text{DTT}]) \quad (\text{Eq. 3})$$

The fitted constant  $k$  provides a measure of the saturable effect of DTT in forced unfolding (Table IV). The fit also yields an apparent specificity constant for DTT,  $K = 1.25$  mM. Both

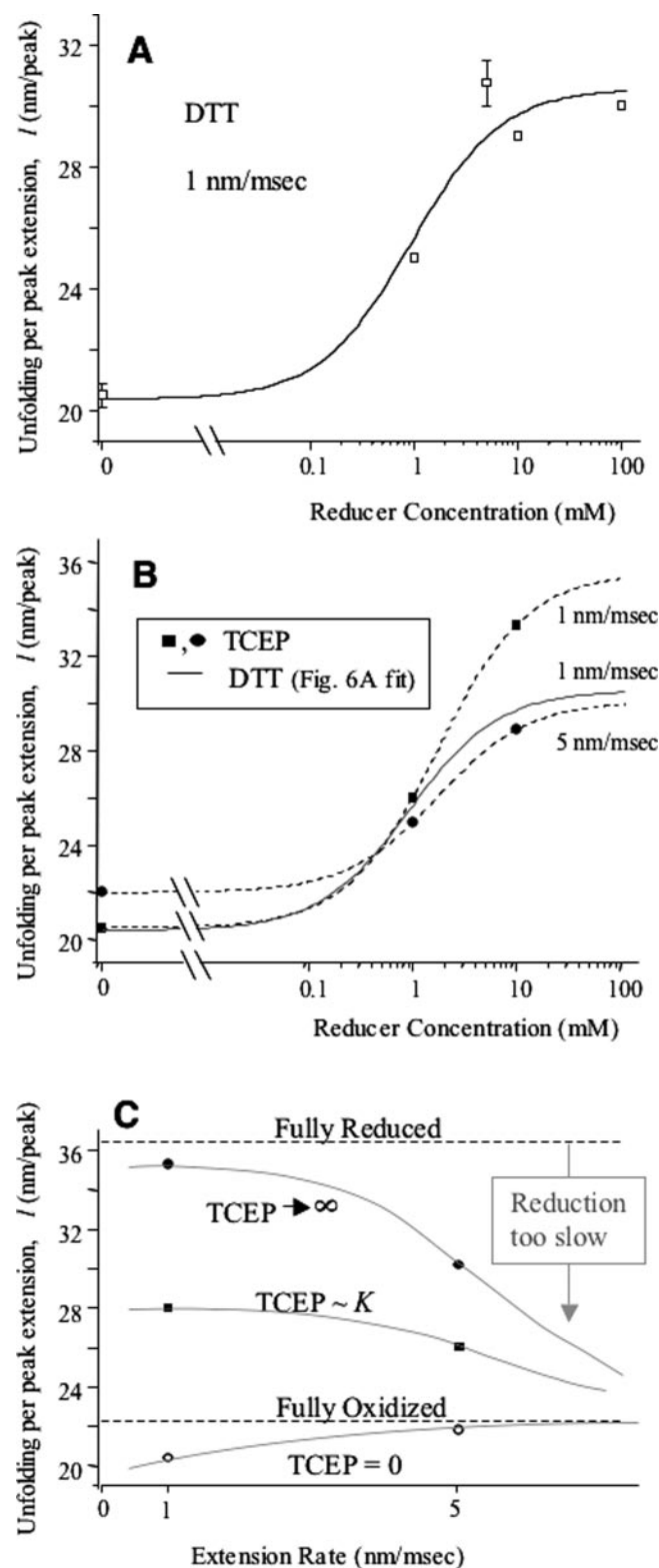


FIG. 8. Plots of unfolding length per peak versus reducer concentration. A, DTT and a chain extension rate of 1 nm/ms. Results are fit with a hyperbolic curve, consistent with Michaelis-Menten kinetics of an AFM reduction-coupled mechanism. B, results for unfolding length ( $l$ ) per peak versus concentration of TCEP (in mM) with fits. C, extension rate-dependent trends estimated from the fits. At high rates, a common asymptote of minimal reduction and maximal extension of the oxidized domains is expected from the data.

folded domains and reducing agent are substrates of the generalized “enzyme,” and the unfolded domains correspond to the product. Fit results for both DTT and TCEP are tabulated in

Table IV together with an expression for a catalytic efficiency  $\Phi = k/K$  to complete the analogy with Michaelis-Menten enzyme kinetics.

The TCEP results (Fig. 8B) compare well with DTT, although TCEP proves slightly more potent with a higher  $\Phi$  at the same extension rate (1 nm/ms). The same conclusion had been reached before from our  $N_{pk}$  statistics in Table III. Fig. 8B further illustrates a decrease in unfolding lengths with increasing extension rate (5 nm/ms). Note that the saturation length,  $l_{sat}$ , for TCEP at 1 nm/ms reaches 35.6 nm, which is in excellent agreement with the maximum tabulated in Table I ( $\langle l^R \rangle = 35.1$  nm).

Importantly, homologous IgCAM domains have already been shown to be inaccessible to DTT and TCEP (up to 10 mM) unless denaturant is used (6). Thus, the enzymatic activity of the AFM force indeed motivates the saturating Michaelis-Menten fits (Equation 3) of Fig. 8. Although it is difficult to know whether  $l_{sat}$  for TCEP and DTT should be considered significantly different, similar catalytic efficiencies  $\Phi = 8\text{--}9$  nm/mM (at the same extension rate) are suggestive of reduction processes that are more similar than different.

#### DISCUSSION

Fig. 8C provides a concise summary of the key experimental results. At low extension rates and high reducing agent, the unfolding length of a domain is nearly the maximum allowed. Lower reducing agent reduces this length, and so does high extension rate. In the limit of very high extension rate, reduction is simply too slow to occur during extension. The common limit at high extension is the oxidized state. SMD confirmed at least that the core disulfide is accessible extremely early in the unfolding trajectory (Fig. 3). A more complete but simpler model of the coupled unfolding-reduction kinetics is presented below.

*Energy Landscape for Reaction Coordinate Monte Carlo Simulations*—To achieve “domain-by-domain” unfolding of the Ig domains in VCAM, each domain needs to resist unfolding up to a characteristic force. Sustained force accelerates the process by lowering the energy barrier between the native and a completely stretched state and also makes the completely stretched state the more stable one. Under reducing conditions, a higher energy barrier for full unfolding becomes accessible (Fig. 9A). In order to predict the mechanical stability of any particular protein domain, its free energy is described as a function of the spatial coordinates of stretching as shown in Fig. 9B. This sketch can be amended to suggest refolding energetics once the protein is relaxed after extension.

Based on the one-dimensional energy landscape of Fig. 9A and kinetic Monte Carlo methods introduced by others for forced unfolding (14), unfolding traces of VCAM were simulated while also accounting for the disulfide bond reduction reaction and detachment from the surface. Our goal was to estimate  $k_{int}$  of Equation 2. In the case of oxidized state simulations, the probability of unfolding for each of the domains was calculated at each time step using  $P_{unfolding} = \Delta t/t_u$ , with  $\Delta t$  specified (to keep  $P_{unfolding}$  always less than 1.0) and unfolding time  $t_u$  dependent on force per the “Bell” factor  $\exp(-fx_u/k_bT)$ .  $x_u$  is an adjustable length scale (equal to 1.6 nm) (14, 32). The force-distance or work factor ( $-fx_u$ ) has the role of decreasing the energy barrier just as an enzyme does. In the case of reduction, each domain goes sequentially through four states: (i) completely native or fully folded state  $N$ ; (ii) partially unfolded  $D_1$  until the hidden disulfides are exposed; (iii) reduced and partially unfolded state  $D_2$ ; and (iv) reduced and fully unfolded state  $R$ . Each domain starts in state  $N$  and transforms to the next state depending on the transition probabilities calculated at every subsequent interval for extension.

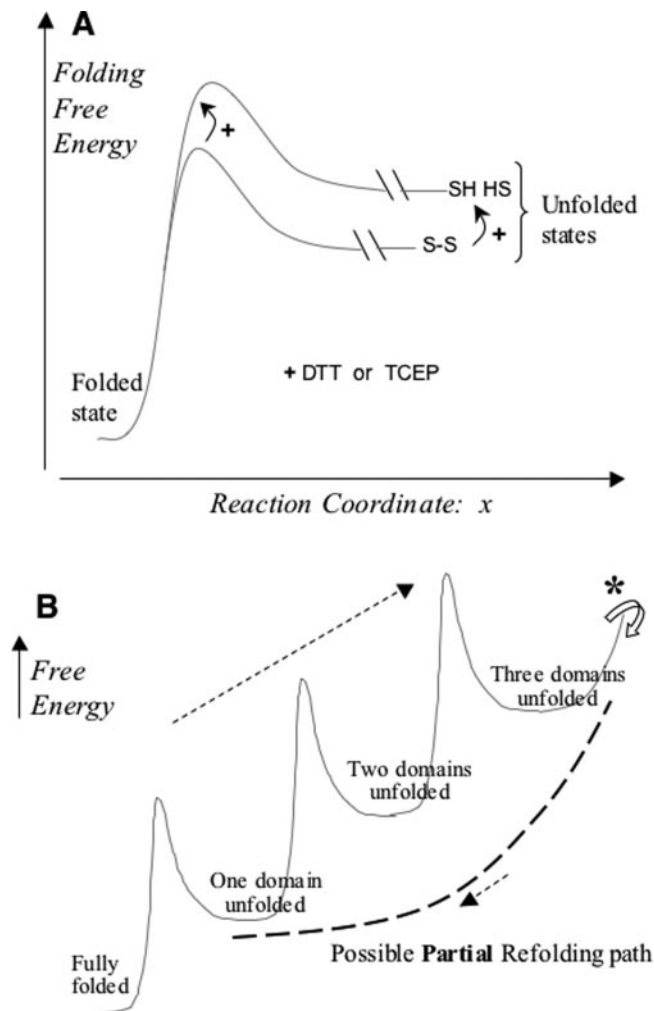


FIG. 9. **Energy landscape for unfolding VCAM.** A, free energy profiles (in the absence of force) for unfolding of a single VCAM domain. The kinetic barriers in these one-dimensional models are overcome in forced unfolding over a distance  $x_u$ . DTT or TCEP (or another reducer for disulfide bonds) is assumed to effectively modulate the barrier height, depending on reactivity and concentration. B, proposed energetics for unfolding-refolding of multidomain VCAM. With extension, as the protein crosses each energy barrier, individual domains are unfolded until there is detachment (\*), or the chain is allowed to relax by reversing the upward motion of the cantilever. In the latter case, unfolding can be repeated.

A sample simulation starts with picking up  $n$  domains ( $d_i$ ,  $i = 1 \dots d_{\text{tot}}$ ) that are all initially in the native state  $N$ . A random number generator picks one of the  $d_i$  domains for a transition to state  $D_1$  until the unfolding probability ( $P_{\text{unfolding}}$ ) exceeds a second random number generated at each extension interval. The domain could maintain this state or change to  $D_2$ . Thus, the reaction scheme simulated is  $N \rightarrow D_1 \rightarrow D_2 \rightarrow U$ . The change to  $D_2$  depends on the reduction probability defined as  $P_{\text{reduction}} = \Delta t/t_{\text{reduction}}$ , where the following is used.

$$1/t_{\text{reduction}} = k_{\text{int}}[\text{DTT}]/(K + [\text{DTT}]) \quad (\text{Eq. 4})$$

If  $P_{\text{reduction}}$  for domain  $d_n$  (in state  $D_1$ ) exceeds a (third) random number, then  $D_1$  transforms to  $D_2$ . It is then mechanically extended to a fully reduced state  $R$ . Chain detachment was modeled with a separate Bell factor  $x_{\text{dis}}$ . The various parameters  $k_{\text{int}}$ ,  $x_u$ ,  $x_{\text{dis}}$ , and a force-free rate  $k_o$  were adjusted so that the simulated sawtooth patterns (Fig. 10A) yielded frequency histograms (Fig. 10B) and concentration dependences for reducer (Fig. 10C) that match the respective experiments (compare with Figs. 5B, 6, and 8B). Note that the simulated saw-

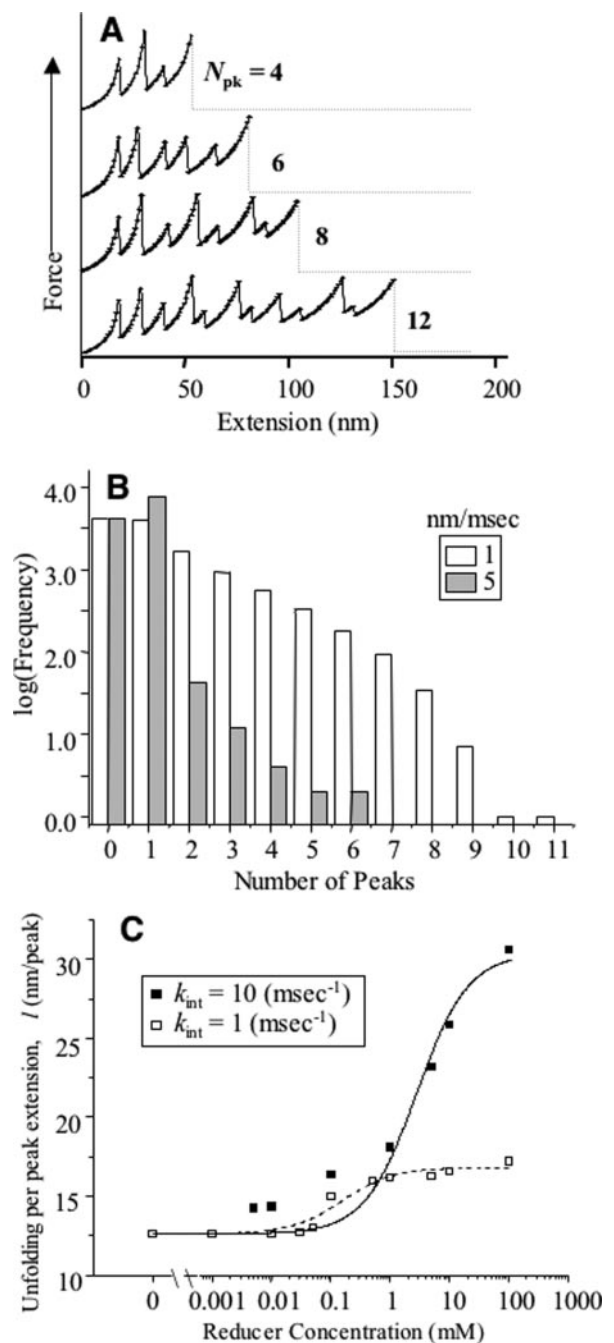


FIG. 10. **Dynamic Monte Carlo simulations of unfolding, for reduced VCAM, were performed as prescribed by Ref. 33 with modifications for both disulfide reduction and detachment probability.** A force-free unfolding rate constant of  $k_u^o = 1 \times 10^{-7} \text{ s}^{-1}$  and a transition state length of  $x_u = 1.6 \text{ nm}$  were used. A force-free detachment rate constant of  $k_{\text{dis}}^o = 1 \times 10^{-9} \text{ s}^{-1}$  and a transition state length of  $x_{\text{dis}} = 1.365 \text{ nm}$  gave good results for  $N_{\text{pk}}$  distributions. A, unfolding curves for VCAM, under reducing conditions with 1 mM TCEP and  $k_{\text{int}} = 10^4 \text{ s}^{-1}$ . B, frequency distributions for the number of peaks observed under reducing conditions with 10 mM TCEP, where the imposed extension rate was either 1 or 5 nm/ms and  $k_{\text{int}} = 10^4 \text{ s}^{-1}$ . C, plot of total unfolding length per unfolded peak versus concentration of TCEP (in mM) with extension rates of 1 nm/ms. Simulations used  $k_{\text{int}} = 10^3$  and  $10^4 \text{ s}^{-1}$ . The hyperbolic fit performed to both simulation results showed that the experimental  $k$  in Fig. 8A lies between that from simulations for  $k_{\text{int}} = 10^3$  and  $10^4 \text{ s}^{-1}$ .

tooth patterns show a similar irregular spacing or stagger of peaks as do the experiments, although the AFM results certainly include more noise as is typical of single molecule experiments (6). The stagger may have prompted the reader to

conjecture that the stagger in experiments resulted from pulling on two or more chains. The simulations here are certainly for one chain and show stagger, and we have also previously analyzed in Law *et al.* (8) the unfolding of two chains in parallel and concluded that higher forces would clearly result but not any experimentally resolvable stagger.

The rate for the disulfide reduction reaction,  $k_{\text{int}}$ , when the disulfides are sufficiently exposed (per Fig. 3) is determined from these MC simulations to be  $k_{\text{int}} \sim 10^3\text{-}10^4 \text{ s}^{-1}$ . This makes  $\tau_{\text{reduction}} \sim 10^{-4}$  s. Naively, one would have made the estimate  $\tau_{\text{reduction}} \sim k/v$ , where  $k$  is from Equation 3 and  $v$  is the extension velocity. Nonlinearities of forced extension apparently limit the accuracy of such an estimate, however. The rate for disulfide bond reduction observed here in our AFM experiments thus proves to be significantly faster than the second order rate constant for the reduction of the disulfide bond of the  $\beta$  2-microglobulin immunoglobulin domain as reported previously (25, 26). Perhaps DTT is convected into the core as the chain is stretched and solvent is drawn in.

**Biological Implications**—Mechanical stretching of multidomain VCAM demonstrated sawtooth patterns with each peak corresponding to single domain unfolding. Although forces to unfold are small, characteristic core disulfide bonds limit unfolding of Ig-CAM domains. This modular elongation mechanism for VCAM might prove a general feature for providing toughness before two adherent cells detach. The inaccessibility of disulfide bonds to various reducing agents was established by wash-in experiments with iodoacetamide, proving that no reduction and/or unfolding occurred on the mica surface before chain extension.

Force is a natural measure of how well two interacting molecules are attached to each other, and the function of CAMs depends on the force to which they are subjected. Multiple domains mean multiple chances to unfold. Although many diseases are related to a malfunction of such molecular recognition processes, no reports of VCAM mutants and pathologies have yet been reported, which is perhaps revealing of the structural integrity of VCAM. A detailed understanding of molecular binding forces among various ligand-protein contacts is important to knowing how force might modulate signaling through VCAM-integrin interactions (34). Cell adhesion experiments under simulated blood flow carried out in successive solutions of a physiological reducing agent (*e.g.* glutathione) followed by iodoacetamide and buffer solution could be performed on VCAM-expressing cells to ascertain the extent of

*in situ* reduction during adhesion. The results here establish a foundation for such cell level studies that address the broader issue of whether forced unfolding occurs biologically.

## REFERENCES

- Kreis, T., and Vale, R. (1999) *Guidebook to the Cytoskeletal and Motor Proteins* Oxford University Press, New York
- Reif, M., Gautel, M., Oesterhelt, F., Fernandez, J. M., and Gaub, H. E. (1997) *Science* **276**, 1109–1112
- Zlatanova, J. (2003) *J. Biol. Chem.* **278**, 23213–23216
- Uyeda, T. Q. P., Abramson, P. D., and Spudich, J. A. (1996) *Proc. Natl. Acad. Sci. U. S. A.* **93**, 4459–4464
- Sahaf, B., Heydari, K., Herzenberg, L. A., and Herzenberg, L. A. (2003) *Proc. Natl. Acad. Sci. U. S. A.* **100**, 4001–4005
- Carl, P., Kwok, C.H., Manderson, G., Speicher, D.W., and Discher, D.E. (2001) *Proc. Natl. Acad. Sci. U. S. A.* **98**, 1565–1570
- Oberhauser, A. F., Marszalek, P. E., Erickson, H. P., and Fernandez, J. M. (1998) *Nature* **393**, 181–185
- Law, R., Carl, P., Harper, S., Dalhaimer, P., Speicher, D. W., and Discher, D. E. (2003) *Biophys. J.* **84**, 533–544
- Elices, M. J., Osborn, L., Takada, Y., Crouse, C., Luhowskyj, S., Hemler, M. E., and Lobb, R. R. (1990) *Cell* **60**, 577–584
- Cybulsky, M. I., and Gimbrone, M. A. (1991) *Science* **251**, 788–791
- Osborn, L., Hession, C., and Tizard, R. (1989) *Cell* **59**, 1203–1211
- O'Brien, K. D., Allen, M. D., McDonald, T. O., Chait, A., Harlan, J. M., Fishbein, D., McCarty, J., Ferguson, M., Hudkins, K., and Benjamin, C. D. (1993) *J. Clin. Invest.* **92**, 945–951
- Li, H., Oberhauser, A. F., Fowler, S. B., Clarke, J., and Fernandez, J. M. (2000) *Proc. Natl. Acad. Sci. U. S. A.* **97**, 6527–6531
- Reif, M., Fernandez, J. M., and Gaub, H. E. (1998) *Phys. Rev. Lett.* **81**, 4764–4768
- Lu, H., and Schulten, K. (1999) *Proteins* **35**, 453–463
- Getz, E. B., Xiao, M., Chakrabarty, T., Cooke, R., and Selvin, P. R. (1999) *Anal. Biochem.* **273**, 73–80
- Han, J. C., and Han, G. Y. (1994) *Anal. Biochem.* **220**, 5–10
- Wallace, T. J., and Mahon, J. J. (1964) *J. Am. Chem. Soc.* **86**, 4099–4103
- Nelson, N., Humphrey, W., Gursoy, A., Dalke, A., Kale, L., Skeel, R., and Schulten, K. (1996) *J. Supercomputing Appl.* **10**, 251–268
- Brooks, R. E., Brucoleri, B. D., Olafson, D. J. States, Swaminathan, S., and Karplus, M. (1983) *J. Comp. Chem.* **4**, 187–217
- Lu, H., Israilewitz, B., Kramer, A., Vogel, V., and Schulten, K. (1998) *Biophys. J.* **75**, 662–671
- Humphrey, W., Dalke, A., Schulten, K. (1996) *J. Mol. Graph.* **14**, 33–38
- Evans, E., Berk, D., Leung, A., and Mohandas, N. (1991) *Biophys. J.* **59**, 849–860
- Marszalek, P. E., Lu, H., Li, H., Carion-Vazquez, M., Oberhauser, A. F., Schulten, K., and Fernandez, J. M. (1999) *Nature* **402**, 100–103
- Gozu, M., Lee, Y. H., Ohhashi, Y., Hoshino, M., Naiki, H., and Goto, Y. (2003) *J. Biochem. (Tokyo)* **133**, 731–736
- Kikuchi, H., Goto, Y., and Hamaguchi, K. (1986) *Biochemistry* **25**, 2209–2213
- Marko, J. F., and Siggia, E. D. (1995) *Macromolecules* **28**, 8759–8770
- Al-Maawali, S., Bemis, J. E., Akhremitchev, B. B., Leecharoen, R., Janesko, B. G., and Walker, G. C. (2001) *J. Phys. Chem.* **B105**, 3965–3971
- Rouzina, I., and Bloomfield, V. A. (2001) *Biophys. J.* **80**, 882–893
- Bustanji, Y., and Samori, B. (2002) *Angew. Chem. Int. Ed.* **41**, 1546–1548
- Shao, J.-Y., and Hochmuth, R. M. (1999) *Biophys. J.* **77**, 587–596
- Bell, G.I. (1978) *Science* **200**, 618–627
- Reif, M., Pascual, J., Saraste, M., and Gaub, H. E. (1999) *J. Mol. Biol.* **286**, 553–561
- Wu, C., Fields, A. J., Kapteijn, B. A., and McDonald, J. A. (1995) *J. Cell Sci.* **108**, 821–829